Purdue University

Purdue e-Pubs

Weldon School of Biomedical Engineering Faculty Working Papers

Weldon School of Biomedical Engineering

3-31-2021

Why Abdominal Aortic Aneurysms Rupture: Predicting Pressure and Diameter at Failure

Charles F. Babbs

Follow this and additional works at: https://docs.lib.purdue.edu/bmewp

This document has been made available through Purdue e-Pubs, a service of the Purdue University Libraries. Please contact epubs@purdue.edu for additional information.

Original Research, May 31, 2021

Why Abdominal Aortic Aneurysms Rupture: Predicting Pressure and Diameter at Failure

Charles F. Babbs, MD, PhD

Weldon School of Biomedical Engineering, Purdue University, West Lafayette, IN 47907-2032, USA. E-mail: babbs@purdue.edu

ABSTRACT

Objective: To perform a first-principles biomechanical analysis of the process of aortic aneurysm rupture, based upon the balance of expanding forces from blood pressure and reactive forces from wall elasticity, and to explore new methods for prediction of rupture risk.
Methods: A mathematical model is created to describe the forces acting on a localized, weak patch of aneurysm wall during the cardiac cycle. A method to obtain patient-specific model parameters non-invasively, including incremental Young's modulus, from cine ultrasonic or magnetic resonance images is proposed.
Results: Pre-rupture integrity of an aneurysm is maintained by the balance between the expanding forces and the reactive elastic forces acting upon the aneurysm wall at its weakest point. Rupture happens when the diameter expands to a critical level, at which any further expansion causes expanding force to increase more than reactive force, producing a runaway increase in size. Using the prevailing systolic/diastolic blood pressure and the pulsatile expansion of the aneurysm, as observed by ultrasonic sector scanning, one can calculate the patient-specific force balance and the critical systolic blood pressure and diameter at failure, assuming a given upper limit of systolic blood pressure. Comparing these calculated values with the measured ones provides two indices of rupture risk. In general, greater than 10-percent pulsatile expansion during clinical testing signals a dangerously low margin of safety.
Conclusions: The proposed method of noninvasive and low-cost risk stratification may be especially important when resources for elective surgery are limited, as in the current and future pandemics. Future clinical studies can be done with existing equipment and protocols, including cine ultrasonic sector scans and multi-institutional databases.

Key words: biomechanics, distensibility, elective repair, failure criteria, impending rupture, mechanics, noninvasive, pathogenesis, patient-specific, rupture risk, stiffness, wall stress

INTRODUCTION

New techniques are needed to better assess when the risk of rupture of an abdominal aortic aneurysm (AAA) justifies the risk of repair[1, 2], including better methods for estimating patient-specific aneurysmal wall properties[3]. This paper presents a potential new solution to an open problem in biomechanics[1-3] -- exactly why and how do abdominal aortic aneurysms rupture, and what are the anatomic and physiologic conditions during which catastrophic failure of the aneurysm wall occurs.

Walls of AAAs are heterogeneous in both thickness and composition, arising as they do, from aged vessels with underlying pathology. There are variable amounts of calcified plaque, intraluminal thrombus[4], elastic fiber content, collagen cross-linking, inflammation[5], degradation of extracellular matrix, apoptosis of smooth muscle cells, and fibrosis[6]. These differences create significant local weak patches[1, 4, 7], especially at the level of greatest diameter. Raghavan et al.[8] found that the failure stress of AAA specimen strips showed large regional variation from 33 to 235 N/cm^2. Wall thicknesses also varied to a similar extent from 0.4 to 4.3 mm. In some aneurysms there is gradual reduction in Young's modulus of stiffness over time[5]. Young's modulus of arterial walls also varies among subjects and is nonlinear[9, 10]. Hence material properties of an aneurysm can vary in both space and time. Accounting for such regional variations should help improve predictions of rupture risk and decisions for intervention[5].

The traditional approach to clinical decision making[3, 11] is that the risk of rupture exceeds the risk of repair when AAA maximal transverse diameter is greater than 55 mm for men or 50 mm for women, based on the work of da Silva and coworkers[12] who found that rupture occurred solely in aneurysms with a diameter > 5.0 cm. However, not all large aneurysms rupture, whereas some small ones may[13, 14]. Not only are false negative predictions of rupture dangerous, leading to catastrophic surgical emergencies, but so too are false positive predictions of rupture. Patients whose AAAs would not naturally rupture over the courses of their lifetimes may be put at unnecessary surgical risk[3].

The 5 cm size criterion is only a guideline. Sonesson[13], for example, found no difference in maximal aneurysm diameter in ruptured AAAs vs. those electively operated on $p = 0.129$. Proposed alternative failure criteria have included maximum principal stress, maximum principal strain and strain energy density at yield[4], local wall strain, radius of curvature, and other variables[15]. Maximal local wall stress, calculated by three-dimensional computer modeling[16] (or by using global measures of size and wall thickness as geometric surrogates of wall stress) has been much investigated[5]. However, peak wall stress has inconsistent association with greater odds of aneurysm rupture in patients with large AAAs[17]. Similarly, aortic aneurysm wall stiffness alone is a poor predictor of impending rupture[13]. In general, various alternative single parameter criteria have not improved prediction.

Vande Geest et al.[7] have introduced a multi-factor rupture potential index, based primarily on thickness, diameter, age, and male vs. female status. Kleinstreuer and Li[18] developed a dimensionless, time-dependent severity parameter based upon eight biomechanical factors involving blood pressure and AAA imaging. These are essentially statistical models. Further progress in accurate prediction of rupture risk may require better understanding of the detailed mechanism of rupture, based upon the underlying physics and biomechanics. Indeed, the exact mechanism of AAA rupture is still unknown. It is unknown whether the wall yields first and then ruptures like ductile material, or if rupture happens suddenly and is more like the failure of a brittle material[4]. Even more than better predictive metrics or statistical models, a whole new theory of the mechanism of rupture is needed to ask and answer fundamental questions about which factors determine catastrophic failure. Ideally, such a theory would include concepts that are mathematically tractable and easy to put into practice.

The present paper describes a fresh, first-principles analysis of failure mechanisms, based upon the balance of forces during stable vs. unstable equilibria. The balance of forces is characterized in cylindrical coordinates for the weak patch of the aneurysm wall, and equilibrium conditions are specified in terms of parameters that can be determined noninvasively. This analysis includes local variation in wall properties. It does not assume uniform wall thickness. Measurement of patient-specific material property values, determined from cine imaging of pulsatile distention during the cardiac cycle, can account for local mechanical effects of stress-shielding of the aneurysm wall by intraluminal thrombus and also for effects of nonlinear variation of wall stiffness with blood pressure and of pathological wall stiffening by varying amounts of calcified plaque and fibrosis. The results lead to a new way of predicting the risk of rupture in animal or human subjects.

Mathematical models are especially appropriate for exploring this particular phenomenon. Clinical observations of the exact moment of aortic aneurysm rupture are rare. Few patients are undergoing continuous electrocardiographic monitoring at the moment of aneurysm rupture. Even if such data were available, it would be difficult to tell retrospectively whether a given elevation of heart rate or blood pressure was a cause of the rupture or a result of acute pain produced by the rupture. A prospective study involving stress tests in humans would be clearly unethical. However, mathematical models of the underlying biomechanics can allow meaningful exploration of the critical conditions leading to catastrophic failure.

METHODS

Analytical model

Figure 1 shows a simple analytical model to explore the essential biomechanics of aneurysm rupture. The model represents a circumferential band of an aneurysm at its greatest diameter and includes a localized weak patch, indicated by dark shading. The band is a thin-walled elastic cylinder of radius, r, and length, L, and wall thickness, h . The inner wall is circular in cross section, consistent with minimization of circumferential strain energy in an elastic tube, and consistent also with typical clinical imaging. However, the wall has continuously varying thickness, including the shaded weak sector, centered at angle $\theta = 0$ on the right. The weak sector may be weak either because it is especially thin, as shown, or because it is especially soft. Pulses of arterial pressure, P, produce periodic radial expansion of the ring at the prevailing heart rate. The vertical N-S (north-south) axis in Figure 1(b) represents the direction of the expanding forces acting on the weak sector.

Here only circumferential or "hoop" forces analyzed. Forces on the wall parallel to the axis of blood flow are considered minimal. These axial forces are ignored because (1) the radial components of axial stress, which would retard expansion, are related to the sine of the angle, ϕ, in Figure 1(a), which is small; (2) although the longitudinal component of axial stress would influence the effective stiffness of the modeled annular segment, the effective stiffness will be directly measured in vivo, as subsequently described, and this effect will be included in the measured result, and similarly for any stress-shielding by intraluminal thrombus; (3) if radial components of tangential stress were significant, they would gradually cause further expansion of the fusiform shape at its distal ends, gradually enlarging the spindle lengthwise and further reducing the axial angle, ϕ, and associated boundary effects.

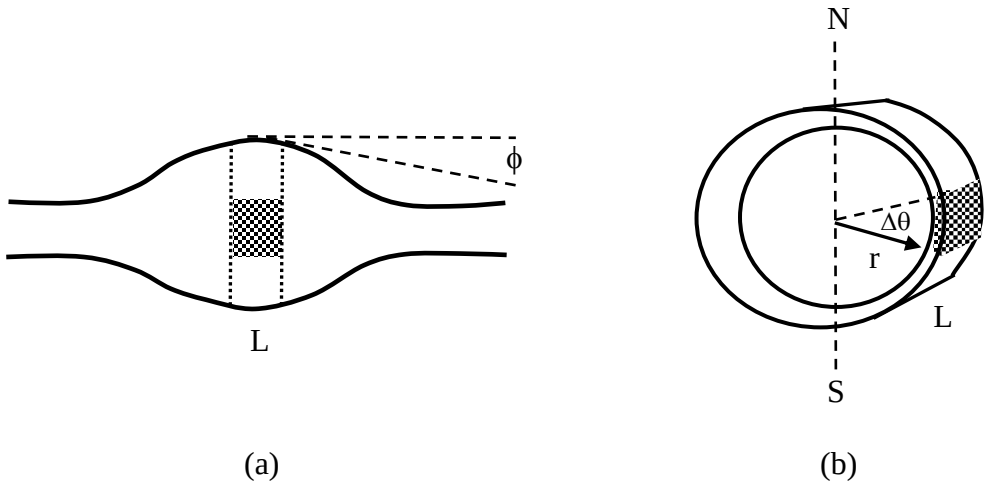

Figure 1. (a) a band-like section of axial length, L, through the widest portion of an abdominal aortic aneurysm, including a weak patch (dark shading). (b) isolated band-like section, including the weak patch of the aneurysm wall. Variables and mathematical notations are defined in the text and in Table 1.

Table 1. Nomenclature

Variable	Definition	Units
E	Young's modulus of elasticity	dynes/cm^2
ε	strain (change in length/reference length)	---
$\hat{f}$	function of measured values $\hat{\lambda}$, $\hat{P}_s$, and $\hat{P}_d$	---
F	force on a weak portion of aneurysm wall	dynes
λ	stretch ratio (stretched length/reference length)	---
L	axial length of modeled cylindrical segment	cm
P	arterial pressure	mmHg or dynes/cm^2
ϕ	slope of aneurysm wall in the axial dimension	radians
π	circle ratio, 3.1416	---
Q	shape factor for nonuniform wall thickness	---
r	radius of aneurysm at its widest diameter	cm
S/D	systolic/diastolic blood pressure ratio	---
θ	angular location on aneurysm wall	radians

Subscripts

d	diastolic blood pressure
s	systolic blood pressure
e	expanding force
r	reactive force
min	minimum wall thickness of weak patch
inc	incremental value

Accents

$'$	local value at weak patch of wall
^	currently measured value
*	future predicted value at rupture

Interplay of forces

Consider the balance of forces on arc length, $r\Delta\theta$, of the wall in a weak patch, having diastolic dimensions, $h_{d,min}$, L, and $r_d\Delta\theta$. The following analysis is based upon the balance of expanding force, F_e , caused by internal pressure and the quasi-static restoring force, F_r , caused by stretch and elasticity of the weak patch. F_e is given by the product of the time-varying internal pressure, P, and area, rL, of the equatorial half plane on the side of the weak patch. Here the weak patch is pre-stressed by the force of diastolic arterial pressure, beyond the "toe" region of its stress-strain curve. In this region the incremental Young's modulus of elasticity, E_{inc} , or stiffness of the arterial wall material, represented by the slope of the stress-strain curve over the range of arterial pulse pressure, is approximately constant[1, 6, 19, 20] (See Discussion).

Hence, the total restoring force, F_r , generated by stretching of the weak patch is given by the baseline restoring force at end-diastole plus the force created by additional local strain, ε' , caused by the arterial pulse. The baseline diastolic force equals the product of the diastolic pressure, P_d , and the area on the side of the weak patch, r_dL, over which the pressure acts. The countervailing elastic force includes the diastolic elastic force plus the force created by additional local strain, ε', produced by the arterial pulse, equals the product of Young's modulus, E_{inc} , and local systolic strain, ε', which can be expressed also as $\varepsilon' = \lambda' - 1$ in terms of the stretch ratio, λ', defined as the stressed length divided by diastolic length of the weak patch. All preceding variables and other mathematical notations are defined and summarized in Table 1.

Combining these ideas, the total reactive force

$$F_r = P_d r_d L + E_{inc} h_{min} \varepsilon' L = P_d r_d L + E_{inc} h_{min} (\lambda' - 1) L , \quad (1)$$

where h_{min} is the time-varying wall thickness of the weak patch and $\varepsilon' = \lambda' - 1$ denotes the local strain of the weak patch. This local strain at the thin patch differs by a factor of

$$Q = \frac{\lambda' - 1}{\lambda - 1} \sim 1.5 \quad (2)$$

from the subsequently measured overall circumferential or "hoop" strain, $\lambda - 1$, where the overall stretch ratio, λ, is the ratio of systolic diameter divided by diastolic diameter at the widest part of the aneurysm as seen, for example, on an ultrasonic sector scan. Hence,

$$F_r = P_d r_d L + E_{inc} h_{min} Q (\lambda - 1) L . \quad (3)$$

Note that because E_{inc} , h_{min} , and Q are multiplied together, and do not appear separately, the weak patch being modeled could be weak because of either softening (decreased E_{inc}) or thinning (decreased h_{min} and accompanying changes in Q). Indeed mathematically, the critical weak patch could occur in any sector of the band of Figure 1, including a softer, thicker sector, as well as the thinnest sector.

Now consider acute expansion of the aneurysm with each heartbeat. During this short time there must be conservation of wall volume so that $r_d \Delta\theta h_{d,min} L = r \Delta\theta h_{min} L$. In turn, the time-varying wall thickness, h_{min} , at the thinnest part of the wall must be

$$h_{min} = h_{d,min} \frac{r_d}{r} = h_{d,min} \frac{r_d}{r_d \lambda} = h_{d,min} \frac{1}{\lambda} . \quad (4)$$

Here time-varying radius, r , is the same at the weak patch as it is at other angles, θ, because of circularization of the lumen required to achieve minimum strain energy (in the absence of a local "bleb" seen on medical imaging). So, the total reactive force generated by the weak patch in terms of the local diastolic minimum stiffness × thickness product is

$$F_r = P_d r_d L + E_{inc} h_{d,min} Q \frac{(\lambda - 1)}{\lambda} L , \text{ or} \quad (5a)$$

$$F_r = P_d r_d L + E_{inc} h_{d,min} Q \left(1 - \frac{1}{\lambda}\right) L \,. \quad (5b)$$

Next consider the time-varying expanding force,

$$F_e = P r_d \lambda L \,, \quad (6)$$

acting on the weak patch in the hoop or "N-S" direction, which is a simple linear function of λ. The interplay between expanding and reactive forces, as functions of the stretch ratio, λ, is sketched in Figure 2.

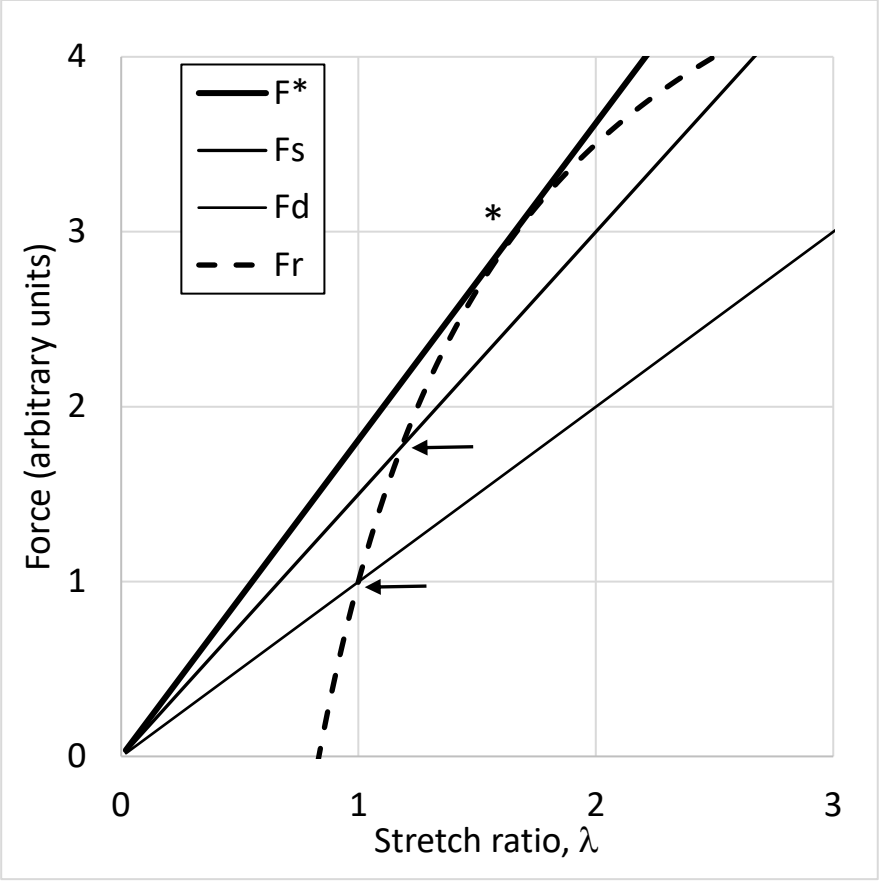

Figure 2. Sketch of expanding and elastic retarding forces acting on a weak patch of a modeled aneurysm wall as a function of the overall stretch ratio λ. Fd indicates force of diastolic blood pressure; Fs indicates force of systolic blood pressure; F* indicates force of systolic blood pressure at failure; Fr indicates reactive elastic force from wall stretch. Lower two crossing points (arrows) are stable equilibria at diastolic and systolic blood pressures. Upper tangent point (*) is an unstable equilibrium and the point of rupture. The illustrative curved function for reactive force in arbitrary units is $F_r = 1 + 5(1 - 1/\lambda)$, similar in form to Equation (5b).

In this context stretch ratio $\lambda = 1$ represents the state of the artery at minimum diastolic pressure. Values $\lambda > 1$ occur during systolic pulsations caused by ejection of the cardiac stroke volume into the aorta and accompanying runoff of blood into the periphery. The reference diastolic radius is denoted r_d and the time-varying stretch ratio is denoted λ, so that $r = r_d\lambda$ during distension. The expanding force, $F_e = Pr_d\lambda L$ (Equation (6)), is directly proportional to λ, as shown by the straight lines in Figure 2. The lower straight line represents diastolic blood pressure. The middle straight line represents systolic blood pressure. The oppositely directed restoring force created by elastic stretch of the weak patch of tube wall is nonlinear and given by Equation (5) corresponding to the dashed curve in Figure 2. This reactive elastic force is described by a downwardly curving function. At the diastolic equilibrium, represented by the stable crossing point at $\lambda = 1$, reactive force equals expanding force.

A perturbation analysis reveals what happens if the stretch ratio is increased or decreased from the end-diastolic equilibrium at $\lambda = 1$ by a small disturbance such as a cough or deep breath. After a small positive perturbation, $\Delta\lambda > 0$, the resulting force difference across the wall becomes negative, as shown in Figure 2, forcing the wall diameter back to the equilibrium position. After a small negative perturbation, $\Delta\lambda < 0$, the resulting force difference across the wall is positive, again forcing the wall diameter back to the equilibrium position. The equilibrium is stable, because wall displacement in either direction results in negative feedback. At normal systolic blood pressure (middle straight line) the same type of equilibrium persists but with a reduced margin on the upward side. There is a stable equilibrium as long as the slope of the reactive force curve is locally greater than the slope of the expanding force curve.

Stretch ratio at failure

Stability persists with increasing expanding pressures until the slope of the expanding force line equals the slope of the reactive force curve at the tangent point, λ^*. This point is the threshold between stability and instability. At λ^* any small positive or negative perturbation, $\Delta\lambda$, or any further increase in expanding pressure, creates a positive force difference across the wall, causing further, runaway expansion. This is the point of catastrophic failure. To specify λ^* exactly, note that when the two curves are tangent at λ^*, the slope of the straight line for expanding force must equal the slope of the curve for retarding force. Differentiating Equations (5b) and (6) with respect to stretch ratio, λ , gives

$$\frac{dF_r}{d\lambda} = \frac{E_{inch_{d,min}}QL}{\lambda^2} \qquad (7)$$

and

$$\frac{dF_e}{d\lambda} = Pr_dL\,. \qquad (8)$$

At the point of failure, λ^*, the systolic blood pressure, $P = P_s^*$, and the two slopes are equal, so that

$$\frac{EQh_{d,min}}{\lambda^{*2}} = P_s^* r_d \, . \qquad (9)$$

Equation (9) defines a failure boundary, $P_s^* \lambda^{*2} = \text{a constant}$, in systolic pressure--stretch space, describing conditions for aneurysm rupture.

Further progress in a practical setting requires knowledge of the lumped constant, $Eh_{d,min}Q$. To evaluate this lumped constant and to estimate the stretch ratio, λ^*, at failure, consider obtaining individualized data from a pre-rupture ultrasound study that measures at $\hat{P}_s$, $\hat{P}_d$ and $\hat{r}_d$ during pulsatile expansion, $\hat{\lambda}_s$, from diastolic to systolic pressures. Here the "hat" accent symbols indicate values determined at the time of the ultrasound study. For a current systolic pressure $\hat{P}_s$, as indicated by the middle curve in Figure 2, we must have expanding force equal to reactive force, or using Equations (5a) and (6),

$$\hat{P}_s \hat{r}_d \hat{\lambda}_s L = \hat{P}_d \hat{r}_d \hat{\lambda}_s L + E_{inc} h_{d,min} Q \frac{(\hat{\lambda}_s - 1)}{\hat{\lambda}_s} L \, , \qquad (10a)$$

which can be put in the form

$$E_{inc} h_{d,min} Q = \hat{P}_s \hat{r}_d \frac{\hat{\lambda}_s (\hat{\lambda}_s - \hat{P}_d / \hat{P}_s)}{\hat{\lambda}_s - 1} \qquad (10b)$$

or

$$E_{inc} h_{d,min} Q = \hat{P}_s \hat{r}_d \hat{f} \, , \qquad (10c)$$

where $\hat{f}(\hat{\lambda}_s, \hat{P}_d, \hat{P}_s) = \frac{\hat{\lambda}_s (\hat{\lambda}_s - \hat{P}_d / \hat{P}_s)}{\hat{\lambda}_s - 1}$, or $\hat{f}$ for short, is an easily computed function of the measured systolic stretch ratio and blood pressure. Thus, the lumped unknown and hard-to-measure variables E_{inc}, $h_{d,min}$, and Q can be determined by a non-invasive ultrasonic sector scan of the widest part of the aneurysm and routine measurement of systolic and diastolic blood pressures with an arm cuff. Knowledge of the exact location and measurement of the minimal wall thickness is not required. In this way it is possible to characterize the curve of reactive elastic force, F_r , as well as the expanding force, F_e , in a patient-specific manner.

The plot of expanding and reactive forces vs. the instantaneous stretch ratio, λ, reveals a stable range of λ values < λ^*, in which equilibrium occurs, and a subsequent unstable range of λ values > λ^*, in which expanding force always exceeds reactive force. The rupture point, λ^*, representing the greatest possible stretch allowing force balance, defines the limit of expansion before rupture. For $\lambda < \lambda^*$ the system is mechanically stable. For $\lambda > \lambda^*$ the system fails catastrophically.

In this case the maximum stretch can be estimated by substituting Equation (10c) in Equation (9)

$$\frac{\hat{P}_s \hat{r}_d \hat{f}}{\lambda^{*2}} = P_s^* \hat{r}_d \tag{11a}$$

or

$$\lambda^* = \sqrt{\frac{\hat{P}_s}{P_s^*}} \hat{f}\,. \tag{11b}$$

Metrics for risk stratification

Critical systolic radius. Using the forgoing approach one can measure the risk of rupture in terms of either the gap between the systolic radius at failure and the current radius, or the gap between the systolic pressure at failure and the current systolic pressure. These values provide indices of risk. Equation (11b) means that for any chosen upper limit of systolic blood pressure, P_s^* , rupture would happen at systolic radius

$$r_s^* = \hat{r}_d \lambda^* = \hat{r}_d \sqrt{\frac{\hat{P}_s}{P_s^*}} \hat{f}\,, \tag{12}$$

where all of the required "hat" variables can be measured in individual subjects. In particular, if systolic blood pressure is assumed to be stable at $\hat{P}_s$, then the systolic radius at failure would be

$$r_s^* = \hat{r}_d \sqrt{\hat{f}}\,. \tag{13}$$

Critical systolic pressure. Also, for the case of stable systolic blood pressure we would expect from Equation (12) that

$$(\lambda^*)^2 = \left(\frac{r_s^*}{\hat{r}_d}\right)^2 = \hat{f}(\hat{\lambda}_s, \hat{P}_d, \hat{P}_s) = \frac{\lambda^*(\lambda^* - \hat{P}_d/\hat{P}_s)}{\lambda^* - 1} \tag{14a}$$

or

$$\lambda^* = \frac{(\lambda^* - \hat{P}_d/\hat{P}_s)}{\lambda^* - 1}\,, \tag{14b}$$

which is a quadratic equation in λ*, namely $\lambda^{*2} - 2\lambda^* + \hat{P}_d/\hat{P}_s = 0$. The relevant solution is

$$\lambda^* = 1 + \sqrt{1 - \hat{P}_d/\hat{P}_s}\,. \tag{14c}$$

To find the burst systolic blood pressure, P_s*, one can combine Equations (11b) and (14c) for λ* to obtain

$$\sqrt{\frac{\widehat{P}_s}{P_s^*}\hat{f}} = 1 + \sqrt{1 - \widehat{P}_d/\widehat{P}_s}\,. \tag{15}$$

Equation (15) can be solved for the failure pressure, P*, after squaring both sides, to obtain

$$P_s^* = \widehat{P}_s \frac{\hat{f}}{2\left(1+\sqrt{\widehat{P}_d/\widehat{P}_s}\right) - \widehat{P}_d/\widehat{P}_s}\,, \tag{16}$$

or, if desired, for the failure pressure ratio $P_s^*/\widehat{P}_s$. All of the terms on the right-hand sides of Equation (12) and Equation (16) can be determined simply, noninvasively, and painlessly in real time. In this way Equations (12) and (16) can be used for risk prediction and risk stratification in patients with abdominal aortic aneurysms.

RESULTS

Using the above analytical approach, one can map either systolic radius (Equation (13)) or systolic blood pressure (Equation (16)) at failure as a function of the stretch ratio measured at the time of study. The dashed curve in Figure 3 indicates the ratio of the future systolic pressure at failure to the measured systolic pressure. This ratio can be interpreted as a safety factor. Increasing stretch ratios measured during the ultrasound study indicate increased distensibility of the aneurysm, either due to softening or due to further thinning of the weak patch. The right-hand ends of the curves in Figure 3 indicate the point of failure. At this point the safety factor equals 1.00, and the failure pressure is the same as the measured systolic pressure. Beyond this point it would have been impossible to do the ultrasonic study.

Similarly, the solid curve in Figure 3 indicates the ratio of systolic diameter at failure to diastolic diameter at the time of the ultrasound study, assuming constant blood pressure in a hypothetical patient with a blood pressure of 120/80 mmHg. This ratio of diameters can also be interpreted as a safety factor. It indicates the maximal size of the aneurysm that could be achieved prior to rupture, if blood pressure remained perfectly stable. At the right-hand end of the solid curve the safety factor is 1.00, indicating that with any further wall softening or thinning, the aneurysm would sprout a leak at its present size.

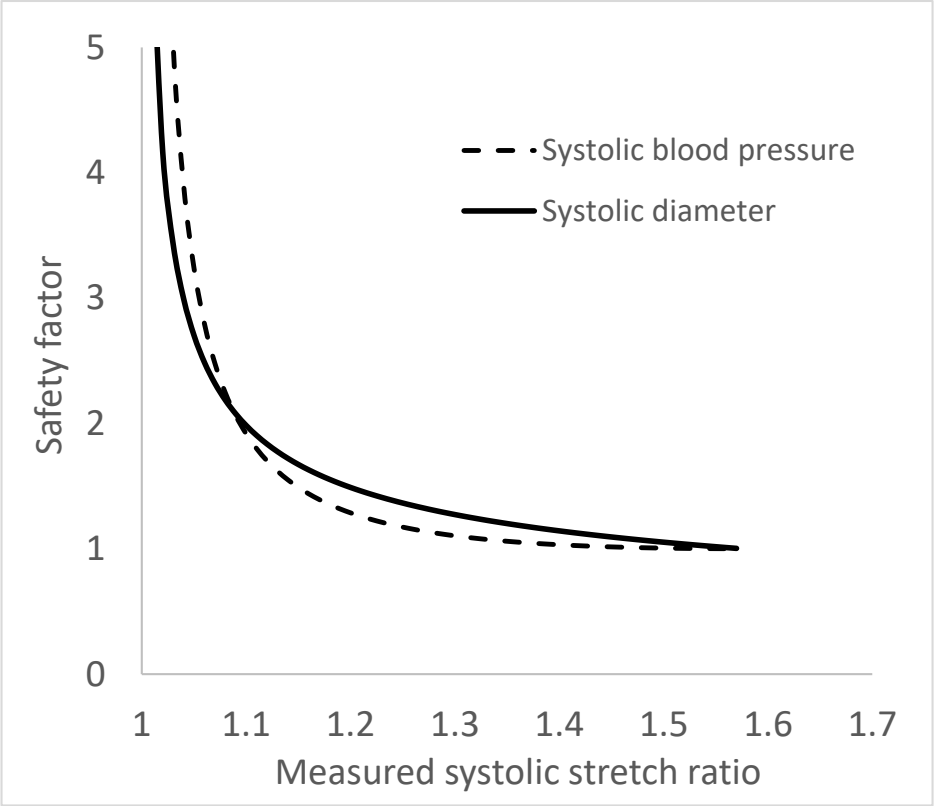

Figure 3. Derived risk indicators for individuals having systolic/diastolic pressure ratio = 1.5 (120/80) as a function of the currently measured stretch ratio.

The differences between the safety factors in Figure 3 and a safety factor of 1.00 can be interpreted as a margin of safety for a particular patient under study. Such differences are shown in Figure 4 in terms of percent. Very large margins of safety to the left indicate that very large increases in either prevailing pressure or prevailing radius would be needed to cause failure. Zero percent margins of safety to the right indicate that the aneurysm would fail immediately with only slight increases in pressure or diameter. In this way an examiner performing a cine ultrasound examination of the widest portion of the aortic aneurysm, together with a simple determination of systolic and diastolic blood pressure with an arm cuff, could obtain indices of impending rupture risk.

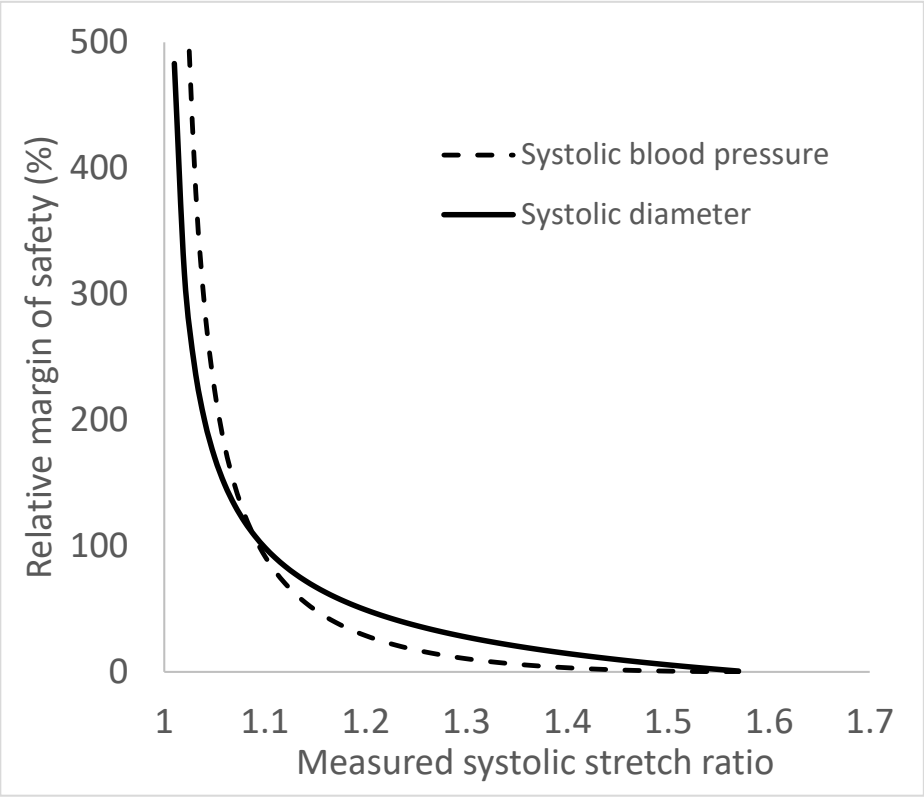

Figure 4. Derived margins of safety for individuals having systolic/diastolic pressure ratio = 1.5 (120/80) as a function of the currently measured stretch ratio.

The particular safety margin curves do differ slightly according to the prevailing ratio of systolic to diastolic blood pressure (S/D), as shown in Figure 5. The systolic margins of safety are greater if the diastolic pressure baselines are lower. The shapes of the curves, as well as interpretations regarding risk, are similar. Systolic to diastolic pressure ratios would tend to bunch near 1.5 in most patients. The modest changes in this parameter cause only modest changes in rupture risk.

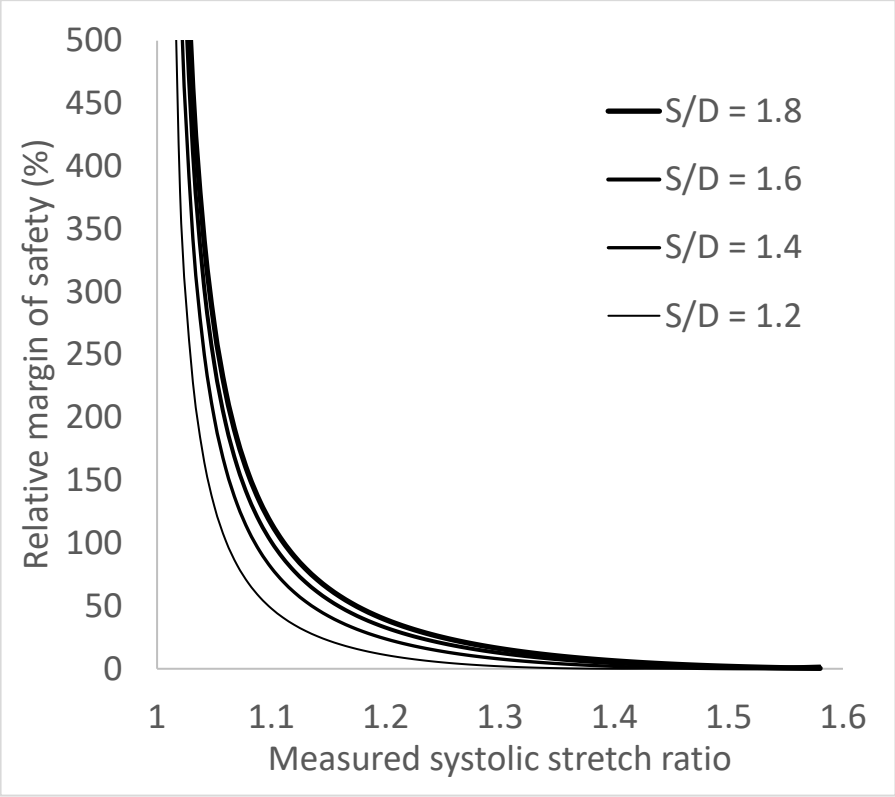

Figure 5. Margins of safety for acute elevations of systolic blood pressure on a stable diastolic pressure baseline as functions of the currently measured stretch ratio and the systolic/diastolic pressure ratio (S/D).

DISCUSSION

To explore basic mechanisms underlying aneurysm rupture, a first-principles analysis is done of expanding forces from internal pressure and reactive forces from wall elasticity that act on the weakest area of an aneurysm wall. These countervailing forces are expressed as functions of the overall systolic stretch ratio, λ , indicating the relative amplitude of systolic radial pulsation. Prior to rupture the wall diameter reaches a stable equilibrium maintained by negative feedback, since reactive force increases more rapidly as a function of λ than does expanding force. However, because the reactive force function curves downward as a function of λ, while the expansive force remains linear; there is a point of instability, λ^*, at which any further expansion causes runaway positive feedback. For any $\lambda > \lambda^*$ expanding force increases faster than elastic force, leading to catastrophic failure of the weak patch.

Based on these underlying biomechanics, the point of failure can be calculated, using Equations (12) and (16), from the prevailing systolic strain and the prevailing systolic/diastolic pressure ratio. Even simpler, if one understands the sharply changing functions relating systolic pulsation and rupture risk, as shown in Figures 3 and 4, then one can use systolic pulsation itself for decision-making purposes, without additional calculation. Generally, if pulsations observed on ultrasonic sector scanning are greater than 10 percent of diastolic diameter, the risk of impending rupture is high. Since there is evidence of progressive weakening of the aortic wall, associated with proteolytic activity and transformation of smooth muscle to amorphous material[1, 3, 5, 15], patients may require periodic re-evaluation; and so simpler, low-cost, noninvasive, procedures for risk assessment are preferable.

Limitations

The present analysis and model may be limited by their simplicity. Possible limitations due to simplifying assumptions include the following:

1. Cylindrical geometry: AAAs may be spherical or saccular; although they are typically fusiform with an average length of 12 cm and average and diameter of 6 cm[4]. Here the cylindrical geometry refers not to the aneurysm as a whole but to a slice through its widest diameter containing a weak patch most likely to rupture. The typically lower wall strength in larger diameter regions[4] justifies the focus of modeling on the widest part. Also, the similar organization of collagen in medial and adventitial layers supports the use of a homogenous, single layer model of wall material, which is characteristic of AAAs compared to normal aorta[19].

2. Simplified boundary conditions: Neglect of axial tension, contact with the vertebral column[21] and contact with other internal organs, could skew predictions.

3. Circular transverse cross section: Circular geometry of sections in the transverse plane is typical but not universal[4, 22]. Complex shapes of cross sections on imaging, including blebs or abrupt discontinuities in curvature, may disallow use of the proposed method without modification.

4. Linear incremental elasticity: Although stress-strain curves are clearly nonlinear over larger ranges of stretch, where a logarithmic fit is most descriptive[6], most of the nonlinearity occurs in the early "toe" regions of the curves at lower values of stress and strain. A linear elastic model is much more reasonable in the range of normal or elevated blood pressures. Such linear behavior above typical diastolic pressures is revealed by experimental measurements (see Fig 2 in [23] Fig 9 in [19] Fig 12 in [1], as well as [6, 20, 24]). In some patients with low-normal blood pressure the "heel" rather than toe region of the stress strain curve could well be included in the needed diastolic to systolic estimate of stretch. Such non-linearity would cause a conservative underestimate of the safety margin and λ^*, but not a gross underestimate, which would occur if the aneurysm wall were not pre-stressed by diastolic arterial pressure.

5. Quasi-static conditions: Dynamic resonance effects could exist to enhance wall strains. Preliminary studies (not shown) indicated that resonance effects can indeed occur in unlikely instances, including individuals with extremely large abdominal girth at cardiac frequencies > 300/min.

The forgoing simplifications are intended to capture the essence of the principal forces that lead to AAA rupture. However, future evaluation, clinical testing, and refinement are clearly needed.

Future directions

The future is bright for testing and refinement of the proposed approach. Necessary imaging techniques are already available and getting better. Today ultrasound is the preferred imaging modality for both AAA diagnosis and monitoring AAA progression[3]. Follow-on clinical research would be relatively low in cost and compatible with existing equipment and protocols at many centers.

The rapid development of ECG-gated, 4D-MRI (three spatial dimensions plus time) may permit better data quality and further progress in the future[25]. ECG gated MR angiography can synchronize with the ECG signal and capture images of the aneurysm at particular times in the cardiac cycle. The resulting noninvasive measurements of systolic pulsations of abdominal aortic aneurysms are technically feasible today, and the quality of imaging is improving. Similarly, 4D-CT angiograms have been used to determine normal cyclic changes in diameter of about 6 percent in the descending aorta[26]. Ganten et al.[27] added ECG gating to their standard CT angiography protocol and segmented the images using an active contour algorithm to obtain systolic vs. diastolic profiles non-invasively; they showed that pulsatile distension was measurable in aneurysms.

Some encouraging preliminary clinical studies of the proposed approach have already been done. Bredahl et al.[28] using ultrasonic scanning found that small aneurysms (unlikely to rupture) showed minimal systolic pulsations ~ 0.7 mm, which is consistent with predictions of the present model. Wilson et al.[29] used ultrasonic scanning in 210 patients to measure AAA distensibility, diastolic blood pressure, and diameter, hoping to find more accurate predictors of rupture risk than diameter alone. They found that an increase in pulsatile distension (decrease in stiffness parameter E_p) was an effective independent predictor of rupture risk.

CONCLUSIONS

There is virtue in being able to determine local elastic properties of abdominal aortic aneurysms in a patient-individualized manner, as suggested here, for the purpose of risk stratification. The present analysis suggests that it is possible to make patient-specific predictions of impending rupture noninvasively. Such predictions can be further tested in clinical settings as well as in laboratory animals both large and small. They may be especially useful when resources for elective surgery are limited, as in the current and future pandemics.

CONFLICTS OF INTEREST

None.

FUNDING

This research did not receive any specific grant from funding agencies in the public, commercial, or not-for-profit sectors.

REFERENCES

1 Niestrawska JA, Viertler C, Regitnig P, Cohnert TU, Sommer G, Holzapfel GA. Microstructure and mechanics of healthy and aneurysmatic abdominal aortas: experimental analysis and modelling. *Journal of the Royal Society, Interface / the Royal Society* 2016; **13**(124) [PMID: 27903785 PMCID: PMC5134013 DOI: 10.1098/rsif.2016.0620]

2 Wassef M, Upchurch GR, Jr., Kuivaniemi H, Thompson RW, Tilson MD, 3rd. Challenges and opportunities in abdominal aortic aneurysm research. *J Vasc Surg* 2007; **45**(1): 192-198 [PMID: 17210410 DOI: 10.1016/j.jvs.2006.09.004]

3 Haller SJ, Azarbal AF, Rugonyi S. Predictors of Abdominal Aortic Aneurysm Risks. *Bioengineering (Basel)* 2020; **7**(3) [PMID: 32707846 PMCID: PMC7552640 DOI: 10.3390/bioengineering7030079]

4 Wang HJ. Noninvasive biomechanical assessment of the rupture potenial of abdominal aortic aneurysms. Electrical Engineering. Pittsburgh PA: University of Pittsburgh, 2002: 257.

5 Humphrey JD, Holzapfel GA. Mechanics, mechanobiology, and modeling of human abdominal aorta and aneurysms. *J Biomech* 2012; **45**(5): 805-814 [PMID: 22189249 PMCID: PMC3294195 DOI: 10.1016/j.jbiomech.2011.11.021]

6 He CM, Roach MR. The composition and mechanical properties of abdominal aortic aneurysms. *J Vasc Surg* 1994; **20**(1): 6-13 [PMID: 8028090 DOI: 10.1016/0741-5214(94)90169-4]

7 Vande Geest JP, Wang DH, Wisniewski SR, Makaroun MS, Vorp DA. Towards a noninvasive method for determination of patient-specific wall strength distribution in abdominal aortic aneurysms. *Ann Biomed Eng* 2006; **34**(7): 1098-1106 [PMID: 16786395 DOI: 10.1007/s10439-006-9132-6]

8 Raghavan ML, Kratzberg J, Castro de Tolosa EM, Hanaoka MM, Walker P, da Silva ES. Regional distribution of wall thickness and failure properties of human abdominal aortic

aneurysm. *J Biomech* 2006; **39**(16): 3010-3016 [PMID: 16337949 DOI: 10.1016/j.jbiomech.2005.10.021]
9 Posey J, Geddes L. Measurement of the modulus of elasticity of the arterial wall. *Cardiovascular Research Center Bulletin* 1973; **11**(4): 83-103
10 Andrew SM, Baker TH, Bocharov GA. Rival approaches to mathematical modelling in immunology. *Journal of Computational and Applied Mathematics* 2007; **205**(2): 669-686
11 Lederle FA, Johnson GR, Wilson SE, Ballard DJ, Jordan WD, Jr., Blebea J, Littooy FN, Freischlag JA, Bandyk D, Rapp JH, Salam AA, Veterans Affairs Cooperative Study I. Rupture rate of large abdominal aortic aneurysms in patients refusing or unfit for elective repair. *JAMA* 2002; **287**(22): 2968-2972 [PMID: 12052126 DOI: 10.1001/jama.287.22.2968]
12 Simao da Silva E, Rodrigues AJ, Magalhaes Castro de Tolosa E, Rodrigues CJ, Villas Boas do Prado G, Nakamoto JC. Morphology and diameter of infrarenal aortic aneurysms: a prospective autopsy study. *Cardiovasc Surg* 2000; **8**(7): 526-532 [PMID: 11068212 DOI: 10.1016/s0967-2109(00)00060-0]
13 Sonesson B, Sandgren T, Lanne T. Abdominal aortic aneurysm wall mechanics and their relation to risk of rupture. *Eur J Vasc Endovasc Surg* 1999; **18**(6): 487-493 [PMID: 10637144 DOI: 10.1053/ejvs.1999.0872]
14 Darling RC, Messina CR, Brewster DC, Ottinger LW. Autopsy study of unoperated abdominal aortic aneurysms. The case for early resection. *Circulation* 1977; **56**(3 Suppl): II161-164 [PMID: 884821]
15 Vorp DA, Vande Geest JP. Biomechanical determinants of abdominal aortic aneurysm rupture. *Arteriosclerosis, thrombosis, and vascular biology* 2005; **25**(8): 1558-1566 [PMID: 16055757 DOI: 10.1161/01.ATV.0000174129.77391.55]
16 Fillinger MF, Marra SP, Raghavan ML, Kennedy FE. Prediction of rupture risk in abdominal aortic aneurysm during observation: wall stress versus diameter. *J Vasc Surg* 2003; **37**(4): 724-732 [PMID: 12663969 DOI: 10.1067/mva.2003.213]
17 Singh TP, Moxon JV, Iyer V, Gasser TC, Jenkins J, Golledge J. Comparison of peak wall stress and peak wall rupture index in ruptured and asymptomatic intact abdominal aortic aneurysms. *Br J Surg* 2020 [PMID: 32996584 DOI: 10.1002/bjs.11995]
18 Kleinstreuer C, Li Z. Analysis and computer program for rupture-risk prediction of abdominal aortic aneurysms. *Biomed Eng Online* 2006; **5**: 19 [PMID: 16529648 PMCID: PMC1421417 DOI: 10.1186/1475-925X-5-19]
19 Gasser TC, Gallinetti S, Xing X, Forsell C, Swedenborg J, Roy J. Spatial orientation of collagen fibers in the abdominal aortic aneurysm's wall and its relation to wall mechanics. *Acta Biomater* 2012; **8**(8): 3091-3103 [PMID: 22579983 DOI: 10.1016/j.actbio.2012.04.044]
20 Xiong J, Wang SM, Zhou W, Wu JG. Measurement and analysis of ultimate mechanical properties, stress-strain curve fit, and elastic modulus formula of human abdominal aortic aneurysm and nonaneurysmal abdominal aorta. *J Vasc Surg* 2008; **48**(1): 189-195 [PMID: 18406563 DOI: 10.1016/j.jvs.2007.12.053]
21 Goergen CJ, Johnson BL, Greve JM, Taylor CA, Zarins CK. Increased anterior abdominal aortic wall motion: possible role in aneurysm pathogenesis and design of endovascular devices. *J Endovasc Ther* 2007; **14**(4): 574-584 [PMID: 17696635 DOI: 10.1177/152660280701400421]
22 Schwartz SA, Taljanovic MS, Smyth S, O'Brien MJ, Rogers LF. CT findings of rupture, impending rupture, and contained rupture of abdominal aortic aneurysms. *AJR Am J Roentgenol* 2007; **188**(1): W57-62 [PMID: 17179328 DOI: 10.2214/AJR.05.1554]
23 Niestrawska JA, Regitnig P, Viertler C, Cohnert TU, Babu AR, Holzapfel GA. The role of tissue remodeling in mechanics and pathogenesis of abdominal aortic aneurysms. *Acta Biomater* 2019; **88**: 149-161 [PMID: 30735809 DOI: 10.1016/j.actbio.2019.01.070]
24 Ambardekar AV, Hunter KS, Babu AN, Tuder RM, Dodson RB, Lindenfeld J. Changes in Aortic Wall Structure, Composition, and Stiffness With Continuous-Flow Left Ventricular Assist

Devices: A Pilot Study. *Circ Heart Fail* 2015; **8**(5): 944-952 [PMID: 26136459 DOI: 10.1161/CIRCHEARTFAILURE.114.001955]
25 Groves EM, Bireley W, Dill K, Carroll TJ, Carr JC. Quantitative analysis of ECG-gated high-resolution contrast-enhanced MR angiography of the thoracic aorta. *AJR Am J Roentgenol* 2007; **188**(2): 522-528 [PMID: 17242264 DOI: 10.2214/AJR.05.1467]
26 Weber TF, Muller T, Biesdorf A, Worz S, Rengier F, Heye T, Holland-Letz T, Rohr K, Kauczor HU, von Tengg-Kobligk H. True four-dimensional analysis of thoracic aortic displacement and distension using model-based segmentation of computed tomography angiography. *Int J Cardiovasc Imaging* 2014; **30**(1): 185-194 [PMID: 24135852 DOI: 10.1007/s10554-013-0307-6]
27 Ganten MK, Krautter U, von Tengg-Kobligk H, Bockler D, Schumacher H, Stiller W, Delorme S, Kauczor HU, Kauffmann GW, Bock M. Quantification of aortic distensibility in abdominal aortic aneurysm using ECG-gated multi-detector computed tomography. *Eur Radiol* 2008; **18**(5): 966-973 [PMID: 18196246 DOI: 10.1007/s00330-007-0833-5]
28 Bredahl K, Eldrup N, Meyer C, Eiberg JE, Sillesen H. Reproducibility of ECG-gated ultrasound diameter assessment of small abdominal aortic aneurysms. *Eur J Vasc Endovasc Surg* 2013; **45**(3): 235-240 [PMID: 23332308 DOI: 10.1016/j.ejvs.2012.12.010]
29 Wilson KA, Lee AJ, Lee AJ, Hoskins PR, Fowkes FG, Ruckley CV, Bradbury AW. The relationship between aortic wall distensibility and rupture of infrarenal abdominal aortic aneurysm. *J Vasc Surg* 2003; **37**(1): 112-117 [PMID: 12514586 DOI: 10.1067/mva.2003.40]